Lawrence Berkeley National Laboratory
Recent Work

Title

PREDICTING THE STRESS-STRAIN BEHAVIOR OF POLYCRYSTALLINE a -IRON CONTAINING HARD SPHERICAL PARTICLES

Permalink

https://escholarship.org/uc/item/0gj769z4

Author

Jones, R.H.

Publication Date

1973-04-01

PREDICTING THE STRESS-STRAIN BEHAVIOR OF POLYCRYSTALLINE α-IRON CONTAINING HARD SPHERICAL PARTICLES

R. H. Jones

April 1973

DISCLAIMER

PREDICTING THE STRESS-STRAIN BEHAVIOR OF POLYCRYSTALLINE α-IRON CONTAINING HARD SPHERICAL PARTICLES

R. H. Jones *

Inorganic Materials Research Division, Lawrence Berkeley Laboratory and
Department of Materials Science and Engineering, College of Engineering;
University of California, Berkeley, California 94720

ABSTRACT

Recent interest in the work hardening of metal crystals

containing a dispersion of hard particles has resulted in analytical

expressions relating the work hardening to strain, particle diameter

and volume fraction as well as other material parameters. In this

study, these models have been used to calculate the tensile stress-

strain behavior of polycrystalline α-iron containing dispersions of

the intermetallic compound Fe_2Ta.

The structural characteristics of the Fe-Ta alloys were

thoroughly evaluated. The particle morphology was measured for random-

ness, mean particle diameter, standard deviation of the particle

diameter, volume fraction and planar interparticle spacing. Also, the

matrix flow strength, composition, crystallographic randomness, dis-

location morphology and grain size were evaluated.

It was found that stress-strain behavior of these poly-

crystalline alloys could be calculated with less than 15% error up to

true plastic strains of 5% using a work hardening model proposed by

Ashby.[3] An error of 0% was obtained for the alloy with the lowest

* Present address: Westinghouse Electric Corporation, Research and
Development Center, Churchill Borough, Pittsburgh, Pa. 15235

volume fraction of second phase at this strain. Above 5% true plastic

strain the work hardening due to the presence of particles was

saturated such that further deformation was similar to that without

particles.

I. INTRODUCTION

For a number of years the only model describing the work hardening of metal crystals containing a dispersion of hard particles was that proposed by Fisher, Hart and Pry.[1] Recently proposed work hardening models for dispersion strengthened alloys include a revised FHP theory by Hart[2], a model proposed by Ashby[3] based on the generation of secondary dislocation loops and a model proposed by Hirsch and Humphreys[4] based on the self hardening of a slip line by rows of loops generated by glide dislocations. The emphasis on understanding the yielding mechanisms in two phase alloys justifiably preempted efforts to understand work hardening mechanisms; however the recently proposed work hardening models have greatly increased our understanding of dislocation-particle interactions. Further work to better characterize dislocation-particle interactions, to refine and establish the limitations in the present models and develop new models is needed. This understanding is desirable because of the potential to design the stress-strain behavior of alloys for post yielding and in optimizing the particle morphology of alloys used in the cold worked condition.

The objective of this study was to demonstrate the effectiveness of existing yielding and work hardening models for predicting the stress-strain behavior of engineering type materials. Alloys of

iron and tantalum containing dispersions of up to 5 vol. % of the
intermetallic compound Fe_2Ta were used for this study. This alloy
system was well suited for this analysis because of the following
characteristics:

1. Hard phase in a soft matrix

2. Equiaxed shaped particles

3. Large volume fraction of second phase (5%)

4. Untextured polycrystalline matrix

5. Low interstitial content

6. Grain boundaries free of particles

Although this alloy is not a commonly used engineering alloy, it is
structurally similar to spheroidized mild steel. It is hoped that this
study represents a step towards applying work hardening models to more
complex polycrystalline alloys.

II. EXPERIMENTAL TECHNIQUES

A. Alloy Production and Heat Treatment

Iron alloys with tantalum concentrations of 0 at. % to 2.0 at. % were cast from 99.95% purity electrolytic iron (Glidden A-104) and 99.9% initial purity tantalum rod. The tantalum rod was given a three pass zone refining treatment prior to use. An induction furnace was used for preparing the ingots with the iron and tantalum held at $1750^{\circ}C$ under argon for 30 minutes prior to pouring.

The ingots were form rolled at $1000^{\circ}C$ from 1.25 in. diameter down to 0.50 in. square rods. Tensile specimens were machined from the square rods, encapsulated in quartz and solution treated for 1 hour at $1400^{\circ}C$, quenched into $45^{\circ}C$ water and then aged in a molten salt bath for 1 hour at $700^{\circ}C$. Grain refinement and spheroidization of the Laves phase was accomplished by heating the samples to $1100^{\circ}C$. The effect of this transformation on the structure and properties of Fe-Ta alloys has been reported by R. H. Jones et. al.[5] During this treatment the samples were enclosed in protective stainless steel bags after which the surfaces were ground to remove any surface reaction products and to assure a uniform cross-section. Surface deformation resulting from the grinding operation was relieved by a 30 minute anneal at $800^{\circ}C$. A schematic of the heat treating schedule is shown in Fig. 1.

B. Alloy Analysis

The equilibrium volume fraction of phases present in the Fe-Ta alloys was determined with the aid of an electron beam micro-probe analyzer and the application of the lever arm principle as proposed by Waldman et. al.[6] and stated below:

$$f = I_T - I_\alpha / I_{Fe_2Ta} - I_\alpha \quad\quad (1)$$

where f is the volume fraction of second phase and I is the intensity of a characteristic X-ray line for tantalum. The use of this technique was necessary because of an incomplete Fe-Ta phase diagram and a lack of knowledge about the composition of the Laves phase in equilibrium with α-iron thereby eliminating the bulk residue analysis technique. Also, extraction replicas are not an accurate method of measuring the particle volume fraction because of a variable extraction efficiency between replicas. The total tantalum intensity, I_T, for each alloy was determined with specimens in the solution treated and quenched condition and that for the Laves phase, I_{Fe_2Ta}, with an overaged specimen. The matrix intensity, I_α, was determined by first obtaining the matrix composition by comparing the lattice parameters of single phase and two phase samples of known composition and converting this composition to an intensity with the composition-intensity data obtained from the single phase alloys. It was possible to obtain an intensity measurement for the Laves phase in overaged samples from large grain boundary particles, but an uncertainty about subsurface particles hindered matrix

6

measurements; therefore, this less direct method was required. The lattice parameters were determined with a Norelco X-ray diffractometer using Cu K_α radiation and a crystal monochromator to reduce the flourescent iron radiation.

Particle size distribution and spatial randomness were determined by measuring 200-300 particles which were extracted from the alloys with carbon films. In preparation for extraction, the specimen surfaces were prepared metallographically with at least three etch-polish steps to insure a scratch free surface with a minimum of deformation. Then, the surfaces were cleaned with hot soap and water, rinsed with alcohol, ultrasonically cleaned in an acetone solution, etched, swabbed with hot soap and water and finally rinsed with alcohol and dried. These steps were taken to assure a clean surface prior to carbon coating. The carbon was deposited in a vacuum evaporator, a grid scribed in the carbon layer and extracted in an acetic 10% perchloric acid solution with 25 volts applied across the sample and a stainless steel cathode. An Hitachi HU-125 electron microscope was used to examine the replicas with a calibrated carbon grating produced by E. H. Fullman Co. used to calibrate the microscope.

Dislocation substructures were evaluated by means of transmission electron microscopy using an Hitachi HU-125 electron microscope at 100 KV. Foils of heat treated material were obtained from slices which had been heat treated, ground to 0.010 in. and chemically thinned to 0.002-0.003 in. thickness in a solution of 85 parts H_2O_2, 10 parts

H_2O and 5 parts of HF. Discs, 3 mm in diameter, were jet polished in an acetic 10% perchloric acid solution at 10 volts. Foils of deformed material were obtained by spark cutting a 0.015 in. slice from the reduced section of a deformed tensile specimen, with the remainder of the treatment similar to the undeformed slices.

An optical metallograph utilizing phase contrast was used to evaluate the grain size and shape. The randomness of the crystallographic grain orientation was determined with the X-ray Laue back reflection technique, with specimens parallel and perpendicular to the form rolling direction.

Experimental stress-strain data was obtained with 0.250 in. diameter tensile specimens with an Instron tensile testing machine at a strain rate of 3×10^{-4}/minute. The load was measured with an accuracy of $\pm$ 0.5% and a sensitivity of 1 kg. The change in length was measured directly from the chart which was synchronized with the crosshead movement. The gage length was established by grinding the reduced section of the tensile specimens with a square fillet and could be measured with an accuracy of 0.5%.

III. STRUCTURAL CHARACTERISTICS OF TWO PHASE Fe-Ta ALLOYS

The plastic flow characteristics of alloys with a dispersion of hard particles are dependent on the properties and morphology of the individual phases. The flow stress of the two phases, the matrix-particle interface properties, the elastic properties of the phases and the shear modulus of the matrix are some of the properties which affect the alloy properties. Morphological characteristics such as the size distribution, shape, randomness and spacing of the second phase, the matrix grain size, dislocation arrangements and randomness of the grain orientations determine the yielding and work hardening properties of two phase alloys.

Following the heat treating schedule shown in Fig. 1, the crystal structure of the matrix phase was always the bcc structure with no evidence of any retained fcc phase. The lattice parameter of the matrix phase was constant for all compositions and was equal to 2.866A. The lattice parameter of the unalloyed iron, heat treated similarly to the alloys, was 2.865 A. Both values are close to that listed by the ASTM Powder Diffraction file for high purity iron of 2.866 A.

Examination of particles, extracted from an overaged Fe-Ta alloy, with the Debye Scherrer x-ray diffraction technique by R. H. Jones[7] confirmed that the Laves phase, Fe_2Ta, is in equilibrium with α iron

at $800^{\circ}C$. The compound, Fe_2Ta, was found to be isomorphous with the hexagonal $MgZn_2$ type structure (C14) with lattice parameters of $a_o = 4.806$ A, $c_o = 7.846$ A and c/a = 1.633. It was also concluded that the Fe-Ta Laves phase was non-stoichiometric and was probably iron rich.

A matrix composition of 0.1 at. % Ta was determined by comparing the lattice parameters of the alloys in the single and two phase conditions. The results of this examination are shown in Fig. 2. A knowledge of the matrix composition was necessary because tantalum is an effective solid solution strengthener in iron.

The particle diameters of two to three hundred particles were measured for each alloy, the number of particles with diameters in groups of 250Å determined and the cumulative probability plotted versus the diameter. Alloys 1, 2, 3 and 4 approximated to normal distributions and alloy 5 to a log normal distribution as shown in Fig. 3. The arithmetic mean is given by the 50% point and the arithmetic standard deviation by the difference between the 50 and 84% points of the normal distriubtion and the geometric mean and geometric standard deviation were determined similarly from the log normal distribution. The geometric mean and geometric standard deviation were converted to arithmetic mean and arithmetic standard deviation. The arithmetic mean diameters, arithmetic standard deviations and volume fractions of Laves phase for alloys are listed in Table 1.

Interparticle spacings on a random plane were calculated from the following relationship:[8]

$$\lambda = 0.5 \left\{ \frac{\pi}{6f} \left(1 + \frac{\sigma^2}{\bar{D}^2} \right) \right\}^{1/2} \bar{D} \qquad (2)$$

where σ^2 is the standard deviation. The center to center spacing as well as the between particle spacing $(\lambda - \bar{D})$ are listed in Table 1.

The spatial randomness of the Laves phase particles was examined by dividing the extraction replica micrographs into squares and counting the number of particles in each square. The probability that a square contained r particles, P(r), was plotted versus the number of particles, r, to obtain the distribution curve. The experimental distribution was compared with the Poisson distribution where:

$$P(r) = \mu^r / r! \ \exp(-\mu) \qquad (3)$$

where P(r) is the probability that a square contains r = 0,1,2,3,. . . particles and μ is the average number of particles. A comparison between the Poisson distribution and the experimentally determined distribution of alloys 3 and 5 are shown in Fig. 4. The close correspondence between the calculated and measured distributions demonstrates the spatial randomness of the particles.

While the stress-strain behavior of a two phase polycrystalline material is strongly dependent on the dispersed phase morphology, it is also affected by the defect density of the matrix

11

phase, the size, shape and crystallographic randomness of the matrix grains and the cleanliness of the boundaries separating these grains. Following the $\alpha \to \gamma \to \alpha$ treatment and an anneal at 800°C, the alloys had a sub-grain structure which was dependent on the particle spacing. The substructures of alloys 3 and 5 are shown in Fig. 5. The sub-grain size of alloys 1 and 5 were determined by lineal analysis and found to be 3200 A and 2000 A, respectively. An ASTM grain size of 4 was measured for all the alloys; however, the boundaries became more irregular with increasing volume fraction of second phase. It was concluded that the greater volume of obstacles to grain boundary movement during the final transformation from γ to α resulted in the increased grain boundary irregularity. Longitudional and transverse specimens of each alloy examined with the Laue back reflection technique revealed that little texturing had occurred during the forming process or subsequent heat treatments.

Evaluation of the plastic flow of two phase polycrystalline material requires grain boundaries which are free of second phase particles and have a minimal precipitate free zone. Grain boundaries without these characteristics would inhibit the measurement of matrix flow properties and would greatly affect the strain continuity at the boundary. Following the heat treatment diagrammed in Fig. 1, the Fe-Ta alloys had grain boundaries which were free of particles and a precipitate free zone. This structure occurred because the peritectoid transformation which was used to refine the grain size was such that

little solubility difference was present between the α and γ phases. Therefore a refined grain structure could be achieved without development of grain boundary precipitates.

IV. YIELDING BEHAVIOR

A. Yielding Theories for Metallic Crystals Containing Hard Particles

Based on the structural characterization of these alloys, a yielding behavior in obeyance to the Orowan yielding model was expected. Orowan[9] proposed that at stresses greater than some critical value a dislocation bowing between non-deformable particles would expand without a further stress increase and bypass the particle. It is necessary that the particles obstructing the dislocation motion withstand the force upon them during the expansion of the loop. Also, if the particle spacing is large substantial dislocation motion and work hardening will occur before dislocation motion is obstructed. Measurement of macroscopic flow behavior would then result in a yield stress larger than that predicted by the bowing mechanism.

Refinements to Orowans original theory have been proposed by Kelly and Nicholson[10] and Ashby[11]. Ashby evaluated the critical configuration for bypass and the variation of the line tension with dislocation character. The approach used by Ashby was to determine the force exerted on a particle by a bowing dislocation, where the force is a function of the angle between the dislocation segments on either side of the particle. Assuming $\theta = 0$, $r_o = 4b$ and substituting $(\lambda - \overline{D})$ to account for large particle diameter, Ashby's relationship for the critical stress of an edge dislocation can be converted to

tensile stresses in polycrystalline material with the aid of the Taylor model[12,13] with the following relationship resulting:

$$\sigma_y = \sigma_o + \frac{MGb\phi}{2\pi(\lambda-\overline{D})} \ln\left(\frac{\overline{D}}{4b}\right) \tag{4}$$

where ϕ accounts for the randomness of the particle spacing.

B. Experimental Results

Of the yielding models mentioned in the prior discussion, the best theoretical-experimental correlation was obtained with equation 4. The value for ϕ was set equal to 0.85 because it was found by Kocks[14] that if the critical bypass configuration is $\theta = 0°$ then the macroscopic flow stress of the random array of particles is 0.85 times the average local Orowan stress. A value of the Taylor factor M of 2.75 was chosen rather then 3.0 because calculations by Hutchinson[15] and Chin and Mammel[16] showed this to be the correct Taylor factor for bcc crystals which deform by pencil glide. The shear modulus, G, for iron was used in all calculations because the 0.1 at. % Ta in solution would not significantly alter this value.

The matrix flow stress was measured with uniaxial tensile specimens of unalloyed iron which had been treated similarly to the alloys. The measured yield strength was 5.5 kg/mm^2 which is close to the 4.8 kg/mm^2 measured by Cuddy and Leslie[17] for titanium gettered polycrystalline iron tested at 22°C. Because of the small tantalum concentration in the matrix of the two phase alloys, the flow stress of unalloyed iron was taken as the matrix flow stress in the two phase alloys.

15

A linear relationship was observed when the 0.2% offset yield strength was plotted versus the particle morphology and dislocation character parameter $\dfrac{1}{(\lambda-\overline{D})} \ln \dfrac{\overline{D}}{4b}$ as shown in Fig. 6. Also, the slope obtained from this plot, 11.1×10^{-5} kg-cm/mm^2, compared favorably with the value for the slope, $0.85MGb/2\pi$, of 9.75×10^{-5} kg-cm/mm^2, as predicted by equation 4. The difference in these two values is only 12%. As expected, the calculated and experimental values of the yield strength agree reasonably well as seen in Table II. An error of 30% is noted for alloy 5, but the other alloys were much closer.

V. WORK HARDENING BEHAVIOR

A. Work Hardening Models for Metallic Crystals Containing Hard Particles

Chronologically, the first model proposed for the work hardening of single crystals containing a hard second phase was by Fisher, Hart and Pry.[1] The FHP model was based on an increased bypass stress necessary because of circular loops which are left as the dislocation bypasses each particle and it assumes that these loops remain in the primary slip plane and exert a shear stress in the matrix which opposes further dislocation motion. The dependence of the flow stress on the volume fractions and the radius of intersection of the particle with the glide plane was stated as follows:

$$\tau_h = \frac{cf^{3/2}NGb}{r} \tag{5}$$

$$\tau_h = (\tau)_{particles} - (\tau)_{without\ particles}$$

where c is a constant equal to about 3, N is the number of concentric loops around the particle, and r is the radius of intersection of the particle with the glide plane. Fisher et al.,[1] also proposed that the increment in flow stress, τ_h, would reach a maximum because the stress build-up around the particle would ultimately fracture the particle. This maximum stress was given as:

$$\tau_{h_{max}} = 3f^{3/2}\tau_c \tag{6}$$

17

Qualitatively the Fisher, Hart and Pry (FHP) model has been supported by experimental results. The prediction of a maximum work hardening increment has been verified in two phase alloys by Hart,[18,19] Safdar and Phillips,[20] Gensamer,[21] and Roberts et al[22]. Also, the work hardening rate predicted by the FHP model and the increase in work hardening with decreasing particle size at a constant volume fraction correspond qualitatively with experimental results. Wilson[23] found that the residual stresses in a plastically deformed two phase alloy were compressive in the matrix and tensile in the particles as expected from the dislocation loop configuration predicted with the FHP model.

Although some aspects of the FHP model have been qualitatively verified, some features have been questioned. The effect of dislocation cross slip cannot be overlooked when considering dislocation-particle interactions; so that, a model based on simple concentric dislocation loops around the particles is not realistic. Dislocation arrangements around particles of plastically deformed material have been shown to be very complex with cell formation observed in copper containing oxides of silica, beryllia and alumina by Lewis and Martin[24] and Goodrich and Ansell[25] in aluminum with a dispersion of alumina. Humphreys and Martin[26] observed prismatic loops with helices the diameter of the precipitates, large jogs and a large density of wide dipoles in plastically deformed Cu-Co single crystals. Thomas and Nutting[27] observed cross slipped dislocations in Al-Cu and Al-Mg alloys and Ashby and Smith[28] observed prismatic loops in internally oxidized Cu-Al alloys. It has been found by Dew-Hughes et al.[29] that Al-Cu single crystals oriented for single

slip instead slipped on many intersecting systems. Ebeling and Ashby[3] found that copper single crystals with up to 1 vol. % of SiO_2 deformed by single slip when oriented for single slip, but the stage I region of the stress-strain curve was replaced by an approximately parabolic stage. The greater volume fraction of second phase in the Al-Cu alloys is thought to account for the more turbulent flow in these crystals when compared to the copper crystals.

At the maximum work hardening increment, the FHP model predicts a steady state number of loops around each particle. The mechanism by which this steady state is maintained is not clear, but it seems unlikely that the loops collapse by shearing the particle which in most cases is an oxide or intermetallic compound. Hart[19] found τ_c to be 0.07 E and 0.3 for Al-Cu and Cu-Cr alloys which for the case of Cu-Cr mean 50-100 dislocation loops surround each particle when steady state conditions exist. Since the elasticmodulus of the matrix would generally be less than the particle, the theoreticl strength of the matrix would be exceeded prior to that of the particle thereby resulting in secondary dislocations being generated rather than particle shear. It is possible that the particle matrix interface may separate; however, this has not generally been observed.

Experimental verification of the FHP relationship has been claimed by Fisher et. al.[1] and Ashall and Evans[30]; however, both tests were with polycrystalline material. The only test of this theory using single crystals was with Al-Cu alloy single crystals by Dew-Hughes and Robertson[29]. The authors found the best linear fit with τ_h plotted versus f/r rather than $f^{3/2}/r$.

In a recent paper, E. W. Hart[2] presented a theory which was intended to alleviate the defects of the original FHP model. In his presentation Hart assumed that work hardening of the matrix proceeds similarly with or without particles, the particles trap loops which raise the critical bowing stress and the Orowan stress is simply additive to the matrix flow stress. The relationship which Hart presented was as follows:

$$\sigma_h = \sigma_y \left[1 + 6c^{1/2}f^{3/4}\left(\frac{G}{\sigma_y}\right)^{1/2} \varepsilon^{*1/2} + 18cf^{3/2}\left(\frac{G}{\sigma_y}\right)\varepsilon^* \right] \quad (7)$$

where σ_h is the difference between the flow with and without particles, c is a constant and ε^* is the tensile glide strain discontinuity about a particle. Since some recovery of the dislocations trapped by particles can occur, the glide strain discontinuity does not equal the homogeneous tensile strain. An approximation that can be made is that

$$\varepsilon^* = \varepsilon \text{ for } \varepsilon < \varepsilon_c$$

where ε_c is the strain at the maximum hardening stress. The constant c in equation 7 depends on Poisson's ratio in the following way:

$$c = 0.509\left\{ 1 + \frac{0.5\nu}{(1-\nu)} \right\}$$

As a correction for nonuniform particle size, Hart proposed that f be replaced with f_{eff} which is assigned a value which makes the calculated and experimentally determined values of σ_h equal at $\varepsilon = \varepsilon_c$.

This empirical adjustment of f has the result of balancing the linear

and parabolic strain terms and hence the shape of the σ_h versus ε

curve as well as the magnitude of σ_h.

In copper single crystals containing a dispersion of SiO_2

particles, it was observed by Ebeling and Ashby[3] that with an increasing

volume fraction of SiO_2 single crystals oriented for single slip de-

formed more homogeneously with more obscure slip line traces, Laue

patterns became blurred and formed Debye rings and finally shape

changes became more typical of a polycrystal than a single crystal.

The observation of dislocation networks around the particles accompanied

these changes in slip behavior. The following relationship best de-

scribed their data:

$$\tau = \tau_y + CG(bf\gamma/\overline{D})^{1/2} \tag{8}$$

where τ is the shear stress required to flow the two phase alloy, τ_y

is the critical resolved shear stress of the two phase alloy and C is

a constant equal to 0.2 to 0.4. Ashby[32,33] later demonstrated that

this type of relationship occurs if it is assumed that work harden-

ing occurs because of the interaction of geometrically necessary dis-

location loops (secondary dislocations) nucleated at the particle-

matrix interface and dislocations moving on the primary slip plane.

The secondary loops are produced to relieve the stress due to slip

on the primary plane. Ashby[3] has stated that the secondary slip model

makes predictions about the rotations of the matrix lattice,

asterism of Laue spots, density of secondary dislocations and the

initiation of cavitation. Primary to the model is the concept that
if particle fracture or cavitation do not occur, secondary dislocations
are geometrically necessary. Hirsch and Humphreys[31] have questioned
the following three assumptions made by Ashby:

1) The secondary dislocation loops are prismatic and
   randomly distributed.

2) The Burgers vectors are random.

3) The secondary dislocation loops are sessile.

A work hardening model based on the selfhardening of a slip
line by rows of loops generated by glide dislocations has been pro-
posed by Hirsch and Humphreys[4]. Above a critical strain, the form of
their relationship is similar to Ashbys. Because of this similarity
and the uncertainty in assigning values to some of the constants in
their relationship, only the Ashby model has been presented. It is ex-
pected that an equivalent experimental fit would be obtained with the
Hirsch and Humphrey model, however, the magnitude of the stress at a
given strain may be subject to greater error.

B. Comparison Between Calculated and Experimental Flow Curves

The tensile stress-strain behavior of polycrystalline iron
containing a dispersion of hard spherical particles of volume fractions
ranging between 0.73 and 5.3 vol. % have been compared with the
stress-strain behavior predicted by equations 5, 7 and 8. Experimental
agreement with the FHP theory in the form of equation 5 and the ob-
servation of a maximum σ_h was observed. Values of σ_h were obtained
by subtracting the stress-strain curve of iron samples treated and

22

tested similarly to the two phase alloys. The values for the volume
fractions and the particle diameters listed in Table 1 were used
for this comparison. The results of plotting σ_h versus $f^{3/2}/r$ are
shown in Fig. 9 where good agreement was observed at values of $f^{3/2}/r$
less than 7×10^{-6} $\overset{o}{A}{}^{-1}$. The maximum values of σ_h obtained in the
two phase Fe-Ta alloys are shown in Fig. 10, however a definitely non-
linear relationship was observed when σ_h (max) was plotted versus $f^{3/2}$.
Since the FHP theory predicts a linear stress-strain relationship[31]
while the experimental stress-strain relationship was non-linear, as
shown in Fig. 11, and because of the previously cited discrepancies
between experiment and the FHP theory, it was concluded that the FHP
theory is not adequate   to describe the stress-strain behavior of the
polycrystalline alloys tested.

Comparison between the experimental stress-strain behavior
and the relationship proposed by Hart[2], as stated by equation 7, was
made with the experimentally determined particle volume fractions and
the effective volume fractions. The values of f, G and σ_y listed in
Table I were used for these calculations. With these particle volume
fractions, equation 7 predicts a flow stress at 5% true plastic strain
of 43 kg/mm^2, 98 kg/mm^2 and 157 kg/mm^2 for alloys 1, 3 and 5, re-
spectively. These values represent errors of 43%, 130% and 170% with
respect to the experimental results. Since the discrepancy was so
great the effective volume fractions were calculated and found to
be 0.19%, 0.25% and 0.40% for alloys 1, 3 and 5, respectively. The
effective volume fractions differ by an order of magnitude from those

23

listed in Table I and cannot represent the fraction of particles

contributing to the work hardening. Since the empirical evaluation of

the particle volume fractions has the effect of shaping the calculated

stress-strain curve and adjusting the stress magnitude, a good fit

with the experimental results was expected and is demonstrated by

the plots shown in Fig. 11. However, the usefullness of equation 7 for

predicting the stress-strain behavior of an alloy is severely limited

by the need to fit the function to the results.

Flow curves have been calculated using Ashbys work hardening

model as expressed by the relationship below:

$$\sigma = \sigma_y + M^{3/2} CG \left(\frac{bf\epsilon}{\overline{D}} \right)^{1/2} \tag{9}$$

The single crystal shear stress-strain relationship as expressed by

equation 8 was converted to a polycrystalline tensile stress-strain

relationship by applying the Taylor model.[12, 13] With the constant

C in equation 12 equal to 0.46 and the values of σ_y, b, f and $\overline{D}$ equal

to those listed in Table I and II, the calculated flow curves shown in

Fig. 11 resulted. The correlation between these curves and the ex-

perimental results is excellent at small volume fractions (alloy 1)

with increasing deviation at larger volume fractions. At a true

plastic strain of 5%, the deviations are 0%, 13% and 14% for alloys 1,

3 and 5, respectively. The results of alloys 2 and 4 are intermediate

between those of 1, 3 and 5.

C. Comments on the Application of the Secondary Work Hardening Model
for Predictions of Uniaxial Polycrystalline Stress-Strain Behavior

The secondary work hardening model proposed by Ashby[3] and

stated for polycrystalline material by equation 9 gave the best stress-

strain predictions with a minimum of empirical fitting. Some empiricism

was used to obtain a value of 0.46 for the constant C in equation 9

while a value of 0.2 to 0.4 was predicted by Ashby. Since Ashby

proposed this model for primary slip only, the value of this constant

may be larger when deformation occurs by multiple slip. Ashby states

that "the precise mechanism by which secondary dislocations obstruct

primary ones changes only the constant......" . Slip on secondary

systems would contribute to the obstruction produced by the punched out

loops and thereby increase the value of this constant. A value of

0.46 seems small when the multiplicity of active slip systems in bcc

crystals is considered.

The work hardening saturation predicted by the FHP theory and

illustrated for the Fe-Ta alloys in Fig. 10 may explain the deviation

between experimental and calculated results at strains greater than 5%.

This deviation from the secondary work hardening model is demonstrated

by Fig. 12 where $(\sigma-\sigma_y)$ is plotted versus $\varepsilon^{1/2}$. Deviation occurs at true

plastic strains between 0.03 and 0.05 as compared to strains of 0.04

and 0.06 for work hardening saturation. Transmission electron micro-

scope studies of deformed tensile specimens were undertaken to determine

whether particle fracture or particle/matrix decohesion contributed to

this change in work hardening behavior. No fractured particles or

separated interfaces were observed in samples strained 20% in tension.

At plastic strains greater than those at which saturation occurs but less than those at which plastic instability occurs, the stress-strain behavior of these alloys is similar to that of a homogeneous poly-crystalline material.

Further support that the secondary work hardening model adequately describes the stress-strain behavior of these alloys at strains less than saturation is given by the linearity of the plots shown in Figs. 12 and 13 and the agreement between the calculated and experimentally determined slopes of these curves as listed in Table II. The slope of the curve plotted in Fig. 13 is 12.5×10^3 kg/mm^2 while the value predicted by equation 9 is 17.8×10^3 kg/mm^2 when C is taken as 0.46.

It is expected that equation 9 would be equally effective in predicting the stress-strain behavior of other polycrystalline alloys containing a dispersion of hard equiaxed particles. Some consideration must be given to the value of C selected but it may be true that C in most polycrystalline alloys is between 0.4 - 0.5. Also, care must be taken to insure that plastic deformation is not localized at grain boundaries as would occur if a wide PFZ was present, that grain boundaries are not cluttered with particles and that the dispersed phase is non-deformable and approximately equiaxed.

VI. CONCLUSIONS

The stress-strain behavior of polycrystalline α iron containing a dispersion of hard spherical particles has been measured experimentally and compared with the behavior predicted by a modified Orowan yielding model and work hardening models proposed by Fisher, Hart and Pry, Harts revised FHP model and Ashby. Alloys containing up to 5 volume percent of the intermetallic compound Fe_2Ta dispersed in polycrystalline α iron were evaluated at room temperature. The temperature and strain rate dependencies were not evaluated since the main objective was to evaluate the accuracies of these models for predicting the stress-strain behavior of polycrystalline material.

It was found that an Orowan type relationship as modified by Ashby satisfactorily described the yield strength as a function of the interparticle spacing and particle diameter. An experimental slope of 11.1×10^{-5} kg-cm/mm^2 and a calculated slope of 9.75×10^{-5} kg-cm/mm^2 were found for this relationship. The calculated and experimental values for the yield strength differed at most by 13% for four of the five alloys tested.

Both the Hart revised FHP work hardening model and Ashby's model based on the generation of secondary dislocations were in good agreement with the experimental data. Harts revised FHP model required the use of empirically obtained values for the particle volume fraction which differed by a factor of

27

10 from the measured volume fraction and therfore is not suitable for predictive purposes. At tensile strains greater than 5%, the work hardening was characteristic of the matrix without particles therefore deviation between the experimental and calculated results based on Ashby's model differed at large strains. A difference of 0%, 13% and 14% was found between the experimental flow strength and that calculated with Ashby's model at 5% true plastic strain for alloys with 0.73, 3.08 and 5.32 volume fraction of second phase, respectively.

While further work is needed to verify the general applicability of these models to other polycrystalline alloys, the results of this study indicate that it is possible to calculate the stress-strain behavior of polycrystalline alloys to some limiting strain. Also, it is evident that a greater understanding of particle-dislocation interaction mechanisms has been made possible by the development of the work hardening models of Hart, Hirsch and Humphreys and Ashby.

REFERENCES

1. J. L. Fisher, E. W. Hart and R. H. Pry: Acta Met., 1953, Vol. 1, p. 336.

2. E. W. Hart: Acta Met., 1972, Vol. 20, p. 275.

3. R. Ebeling and M. F. Ashby: Phil. Mag., 1966, Vol. 13, p. 805.

4. P. B. Hirsch and F. J. Humphreys: Proc. Roy. Soc. Lond., 1970, A.318, p. 45.

5. R. H. Jones, V. F. Zackay and E. R. Parker: Electron Microscopy and Structure of Materials, G. Thomas, Ed., p. 829, Univ. of Calif. Press, Berkeley, 1971.

6. J. Waldman, M. Schwartz and S. Nash: Trans. ASM, 1969, Vol. 62, p. 819.

7. R. H. Jones, V. F. Zackay and E. R. Parker: Met. Trans., 1972, Vol. 3, p. 2835.

8. R. Ebeling and M. F. Ashby: Trans. AIME, 1966, Vol. 236, p. 1396.

9. E. Orowan: Symposium on Internal Stresses in Metals and Alloys, p. 451, The Inst. of Metals, London, 1948.

10. A. Kelly and R. B. Nicholson: Prog. in Matls. Sci., 1963, Vol. 10, p. 336.

11. M. F. Ashby: Phy. of Strength and Plasticity, Ali S. Argon, ed., p. 113, The M.I.T. Press, Cambridge, Mass., 1969.

12. G. I. Taylor: J. Inst. of Metals, 1938, Vol. 62, P. 307.

13. G. I. Taylor: Deformation and Flow of Solids, p. 3 Springer, 1956.

14. V. K. Kocks: Phil. Mag., 1966, Vol. 13, p. 541.

15. J. W. Hutchinson: J. Mech. Phys. Sol., 1964, Vol. 12, p. 25.

16. G. Y. Chin and W. L. Mammel: Trans. TMS-AIME, 1967, Vol. 239, p. 1400.

17. L. J. Cuddy and W. C. Leslie: Second International Conf. on the Strength of Metals and Alloys, p. 253, American Society for Metals, 1970.

18. E. W. Hart: Relation of Microstructure to Properties, p. 95, ASM, 1953.

19. W. R. Hibbard and E. W. Hart: Trans. AIME, 1955, Vol. 203, p. 200.

20. A. M. Safdar and V. A. Philips: Trans. AIME, 1959, Vol. 215, p. 340.

21. M. Gensamer: Trans. ASM, 1946, Vol. 36, p. 30.

22. C. S. Roberts, R. C. Carruthers and B. C. Averbach: Trans. ASM, 1952, Vol. 44, p. 1150.

23. D. V. Wilson: Trans. ASM, 1955, Vol. 47, p. 321.

24. M. H. Lewis and J. W. Martin: Acta. Met., 1963, Vol. 11, p. 1207.

25. R. S. Goodrich and G. S. Ansell: Acta. Met., 1964, Vol. 12, p. 1097.

26. F. J. Humphreys and J. W. Martin: Phil. Mag., 1957, Vol. 16, p. 927.

27. G. Thomas and J. Nutting: J. Inst. Metals, 1957, Vol. 86, p. 7.

28. M. F. Ashby and G. C. Smith: Phil. Mag., 1960, Vol. 5, p. 299.

29. D. Dew-Hughes and W. D. Robertson: Acta Met., 1960, Vol. 8 p. 147.

30. D. W. Ashall and P. E. Evans: Metal Science Journal, 1968, Vol. 2,

    p. 96.

31. P. B. Hirsch and F. J. Humphreys, Physics of Strength and Plasticity,

    A. S. Argon ed., The M.I.T. Press, p. 189, Cambridge Mass., 1969.

32. M. F. Ashby, Phil. Mag. p. 1157, Vol. 14, 1966.

33. M. F. Ashby, Phil. Mag. p. 399, Vol. 21, 1970.

TABLE I. DATA ON AVERATE PARTICLE DIAMETERS, INTERPARTICLE SPACING, VOLUME FRACTIONS AND COMPOSITIONS OF Fe-Ta ALLOYS

Alloy	$\overline{D}$(Å)	σ(Å)	λ(Å)	$\lambda-\overline{D}$(Å)	f(%)	at. % Ta
1	1250	450	5640	4390	0.73	0
2	1575	475	4970	3395	1.44	0.41
3	1825	800	4110	2285	3.08	1.00
4	2300	875	4380	2025	4.14	1.52
5	2050	990	3440	1390	5.32	2.05

TABLE II. SUMMARY OF CALCULATED AND EXPERIMENTAL YIELD STRENGTH AND WORK HARDENING DATA FOR Fe-Ta ALLOYS

Alloy	$\sigma_y \left(kg/mm\right)^2$		%DIFF.	$M^{3/2}CG\left(\dfrac{bf}{\overline{D}}\right)^{1/2}$		%DIFF.
	EXP.	CALC.		EXP.	CALC.	
1	18.8	16.3	-13	75.5	67.8	-10
2	20.0	20.0	0	95.5	84.7	-10
3	28.1	27.7	-4	115.0	115.0	0
4	31.4	31.7	1	112.0	119.0	6
5	32.9	42.9	30	138.0	143.0	4

NOMENCLATURE

$\overline{D}$ Average particle diameter

f Particle volume fraction

λ Mean planar interparticle spacing

σ_o Matrix tensile yield strength

σ_y Alloy tensile yield strength

M Taylor factor

G Matrix shear modulus

b Matrix Burgers vector

τ Shear stress

σ Tensile stress

γ Shear strain

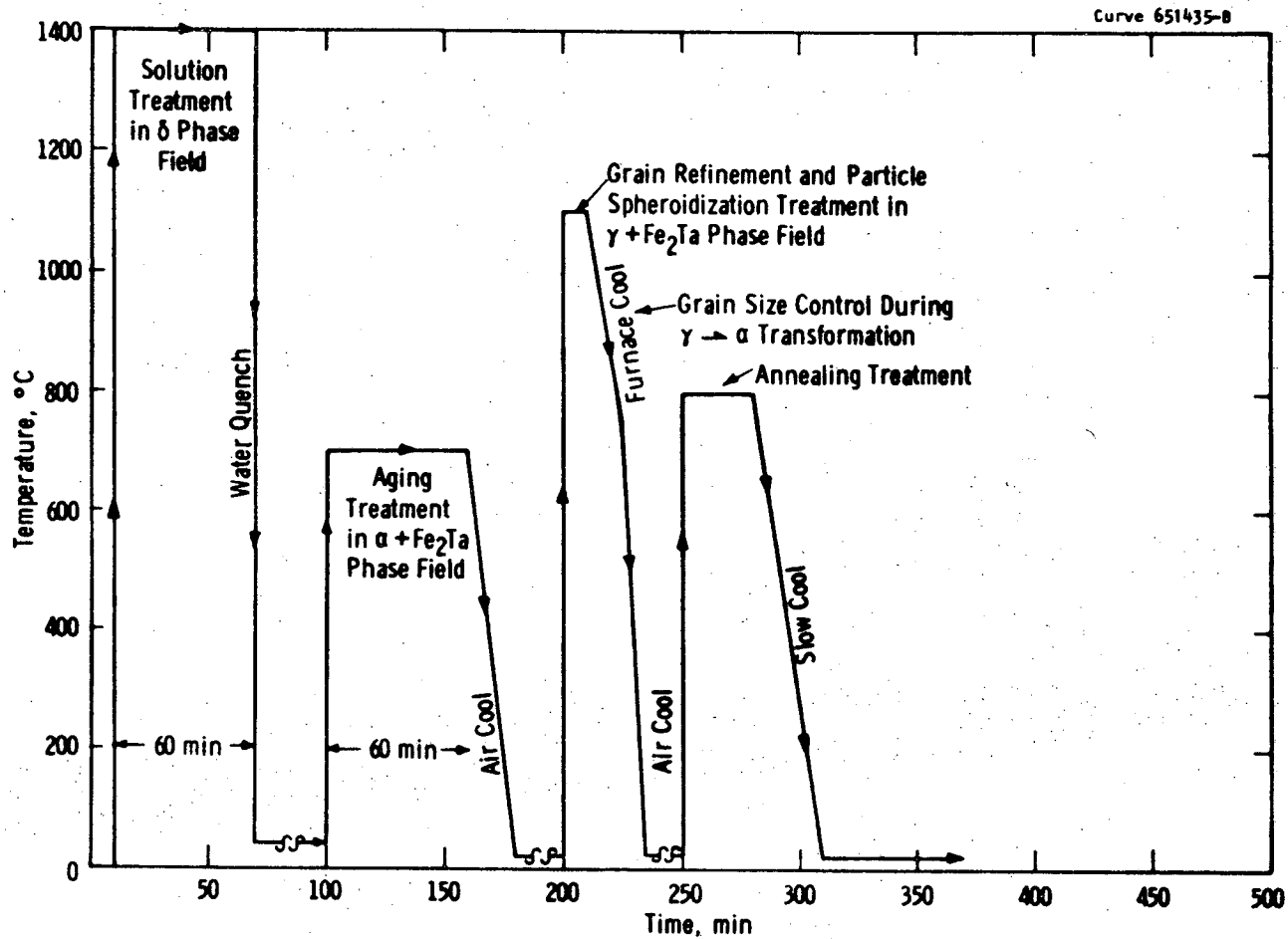ε Tensile strain

ACKNOWLEDGEMENTS

FIG. 1.   Time-temperature schematic illustrating the heat treatment used to obtain a dispersion of spherical Laves phase particles in Fe-Ta alloys.
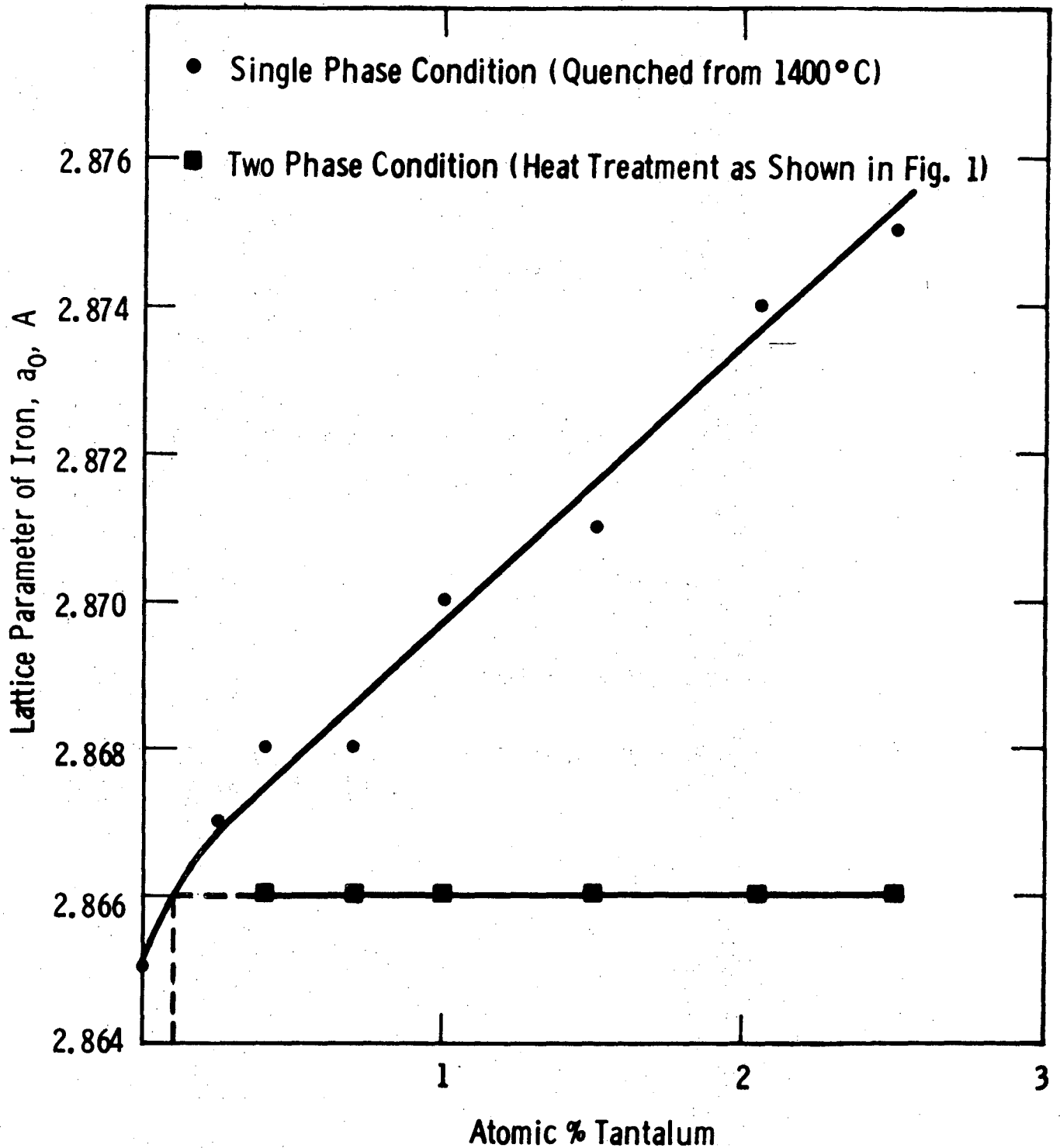
FIG. 2.   Lattice parameter of iron versus atomic percent tantalum for single and two phase Fe-Ta alloys.

FIG. 3.   Cumulative probability versus particle diameter of Laves phase particles extracted from two phase Fe-Ta alloys:

   a) Cumulative probability versus particle diameter plot is typical of alloys 1, 2, 3 and 4.
   b) Cumulative probability versus log particle diameter for alloy 5.

FIG. 4.   The probability, $P(r)$, that a randomly placed square contains r particles versus r, the number of particles per square for alloys 3 and 5 in the two phase condition. Calculated data obtained with the Poisson distribution function and the experimental data from extraction replicas.

FIG. 5.   Transmission electron micrograph showing the Laves phase dispersion and matrix dislocation structure in two phase Fe-Ta alloys subsequent to the heat treatment diagrammed in Fig. 1. a) Alloy 3 ; b) alloy 5.

FIG. 6.   The 0.2% yield stress, σ_y, versus the Orowan parameter, $\ln (\bar{D}/4b)/(\lambda-\bar{D})$, for two phase Fe-Ta alloys.

FIG. 7.   The particle contribution to the work hardening, σ_h, versus $f^{3/2}/r$ for two phase Fe-Ta alloys at true plastic strains of 0.01, 0.02, 0.03 and 0.04.

FIG. 8.   The particle contribution to the work hardening, σ_h, versus the true plastic strain for two phase Fe-Ta alloys.

FIG. 9.   Calculated and experimental true stress-true strain curves for two phase Fe-Ta alloys. Calculated curves based on Harts[2] and Ashbys[3] work hardening models.

FIG. 10. Stress increment $\sigma_f-\sigma_y$, versus $\varepsilon^{1/2}$ for two phase Fe-Ta alloys.
   a) alloys 1, 2 and 3; b) alloys 4 and 5.

FIG. 11. Stress increment $\sigma_f-\sigma_y$, versus the dimensionless parameter, $(bf\varepsilon/\bar{D})^{1/2}$ for two phase Fe-Ta alloys at true plastic strains of 0.01, 0.025 and 0.050.

Fig. 1—Time -temperature schematic illustrating the heat treatment used to obtain a dispersion of spherical Laves phase particles in Fe-Ta alloys
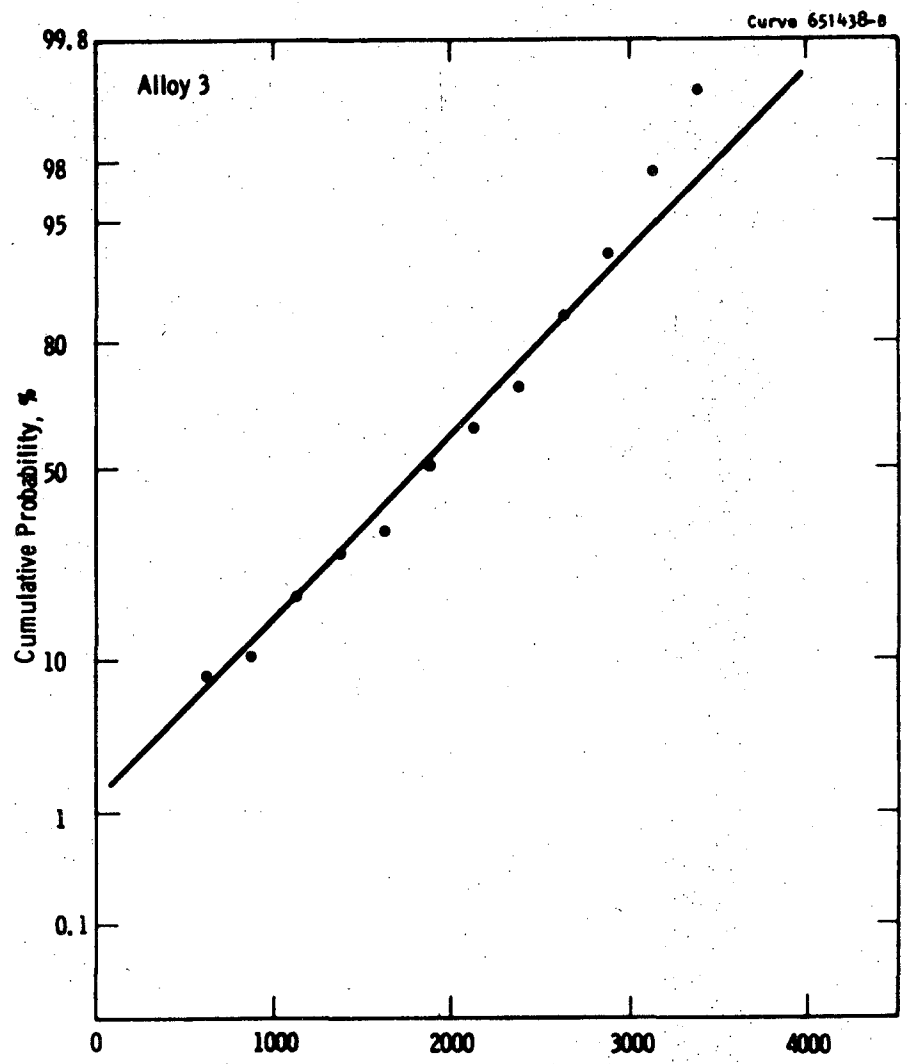
Fig. 2—Lattice parameter of iron versus atomic percent tantalum for single and two phase Fe-Ta alloys.
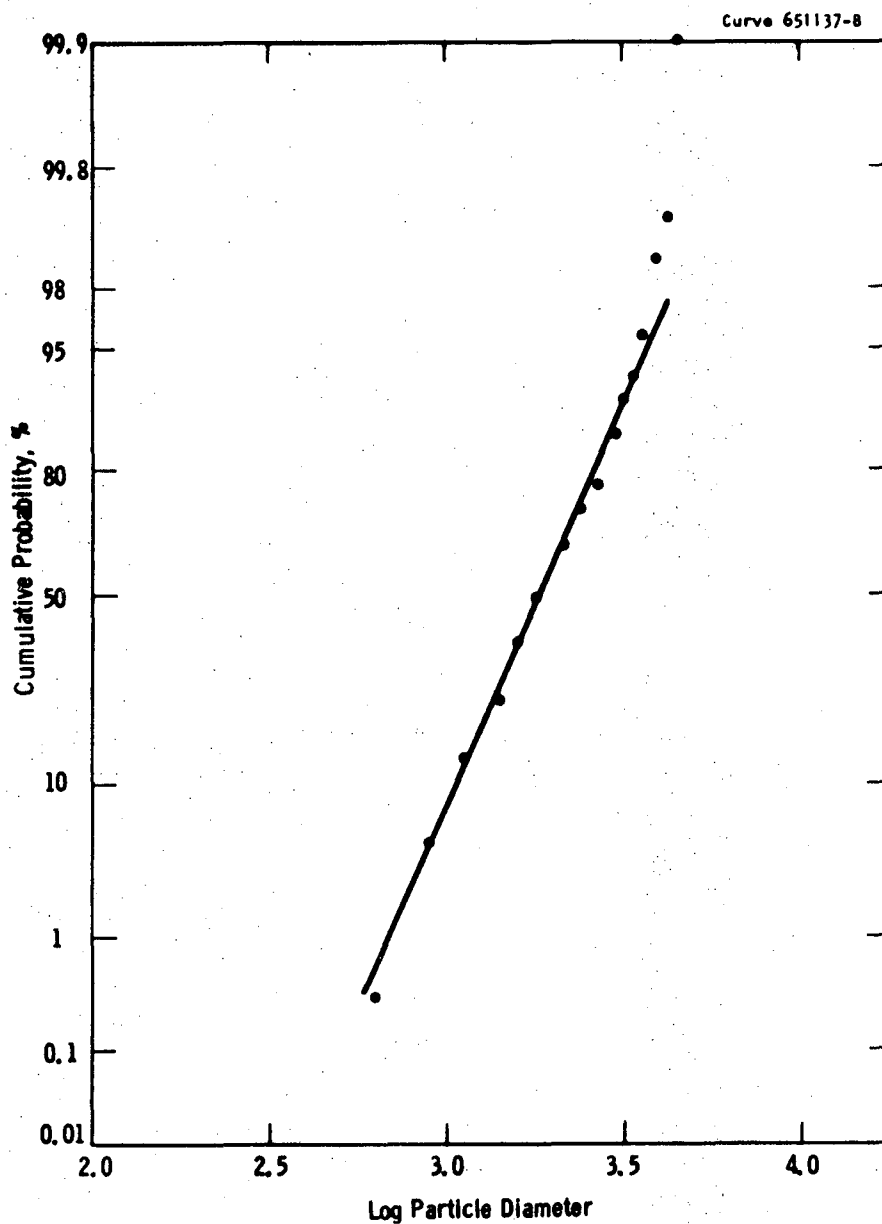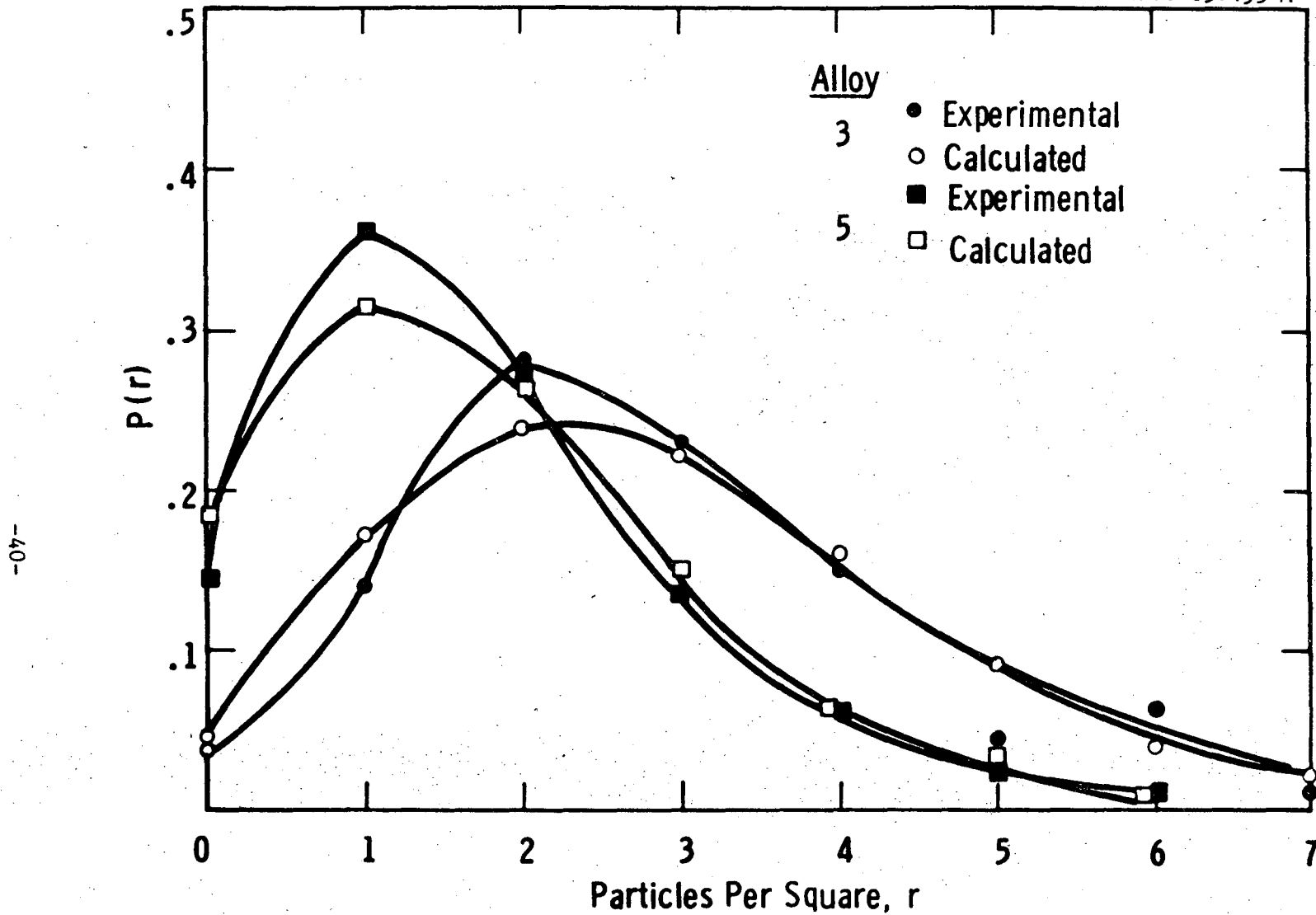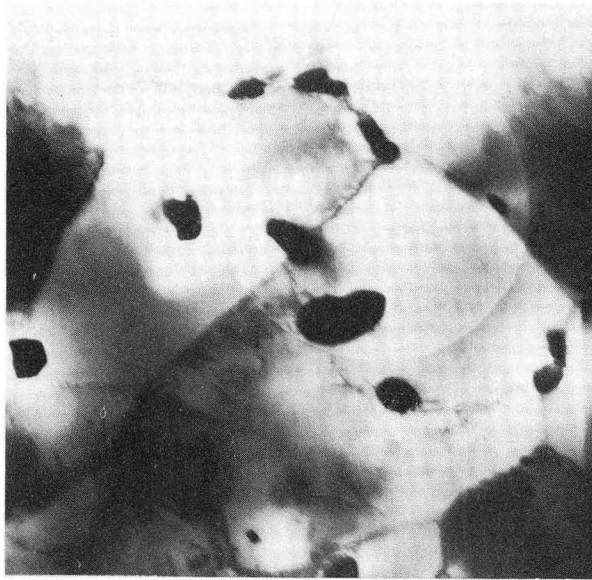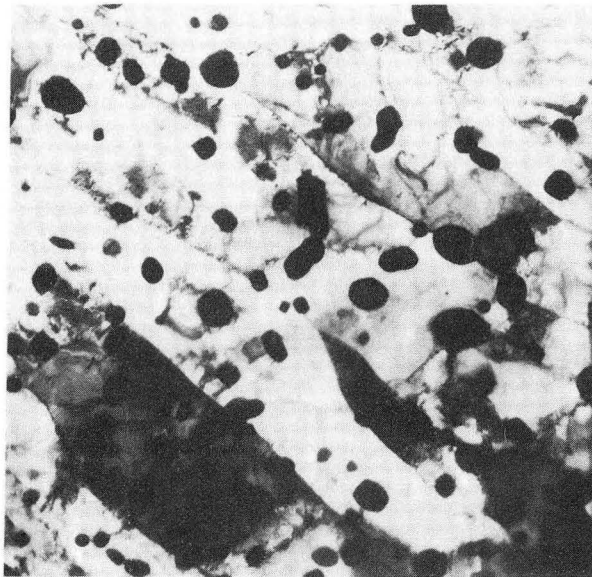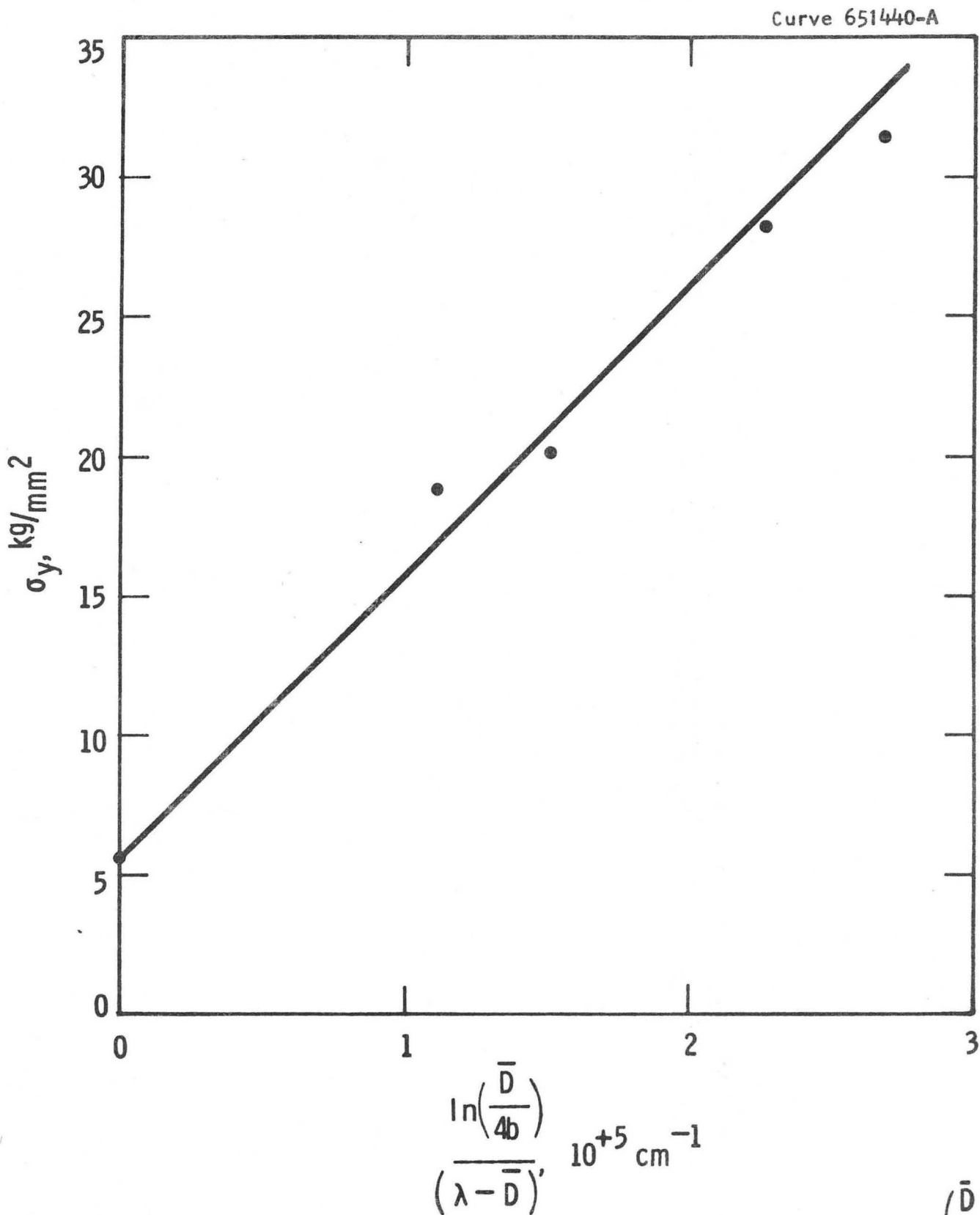
Alloy 3

Particle Diameter, A

Fig. 3a

Fig. 3b

Fig. 3—Cumulative probability versus particle diameter of Laves phase particles extracted from two phase Fe-Ta alloys. (a) Cumulative probability versus particle diameter plot is typical of alloys 1, 2, 3, and 4. (b) Cumulative probability versus log particle diameter for alloy 5.

Fig. 4—The probability, P(r), that a randomly placed square contains r particles versus the number of particles per square for alloys 3 and 5 in the two phase condition. Calculated data obtained with the Poisson distribution function and the experimental data from extraction replicas.

.7 μ

(a)

.7 μ

(b)

Fig. 5—Transmission electron micrograph showing the Laves phase dispersion and matrix dislocation structure in two phase Fe-Ta alloys subsequent to the heat treatment diagrammed in Fig. 1 (a) Alloy 3 (b) Alloy 5

-41-

Fig. 6—The 0.2% yield stress, σ_y, versus the Orowan parameter, $\ln\left(\frac{\bar{D}}{4b}\right)/(\lambda - \bar{D})$, for two phase Fe-Ta alloys.

Fig. 7—The particle contribution to the work hardening, σ_h, versus $f/_r^{3/2}$ for two phase Fe-Ta alloys at true plastic strains of 0.01, 0.02, 0.03, and 0.04.

Fig. 8—The particle contribution to the work hardening, σ_h, versus the true plastic strain for two phase Fe-Ta alloys.

Fig. 9—Calculated and experimental true stress-true strain curves for two phase Fe-Ta alloys. Calculated curves based on Harts[2] and Ashbys[3] work hardening models.

Fig. 10—Stress increment $\sigma_f - \sigma_y$ versus $\varepsilon^{\frac{1}{2}}$ for two phase Fe-Ta alloys (a) alloys 1, 2, and 3 (b) alloys 4 and 5.
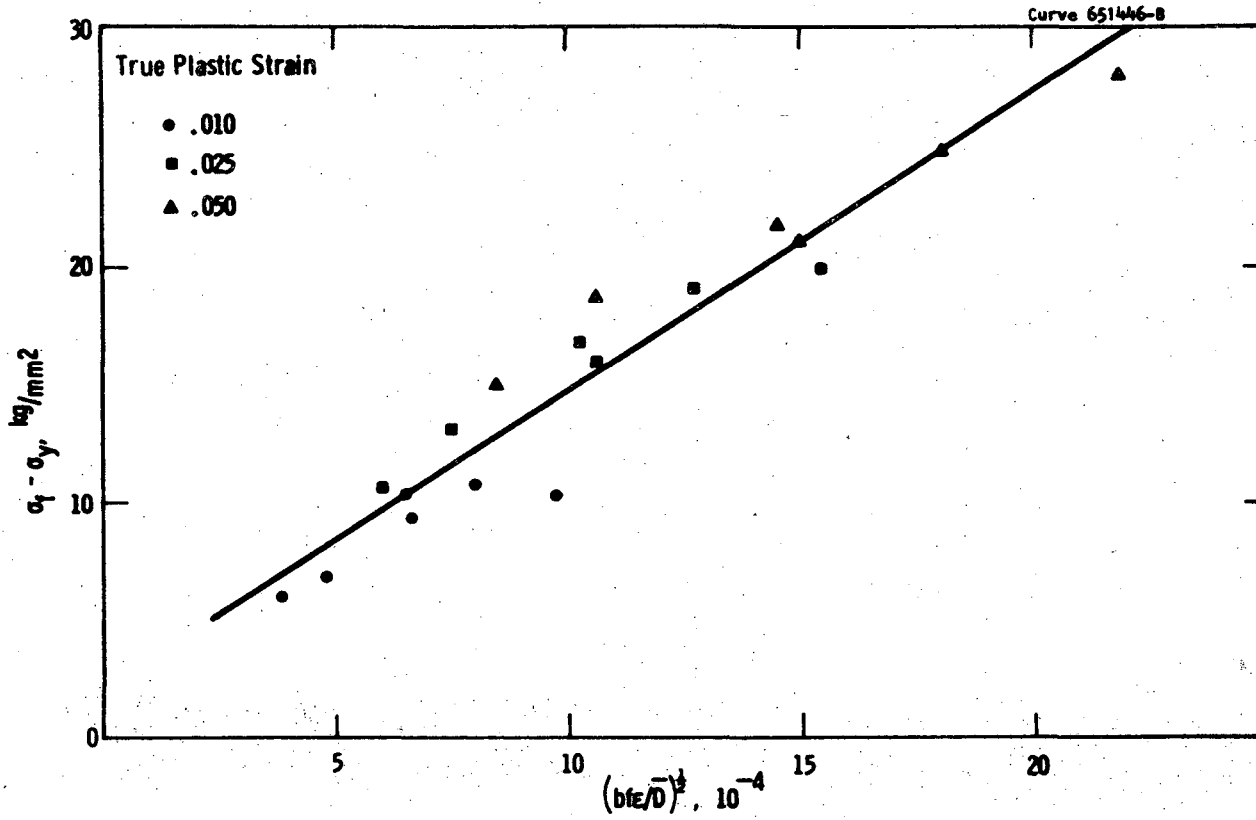
R. H. Jones
m.m. - a.c. 3/1/73

$\sigma_f - \sigma_{y'}$ kg/mm^2

• Alloy 4
■ Alloy 5

25

20

15

10

5

0

0   5   10   15   20   25   30   35

$\varepsilon^{\frac{1}{2}}$, 10^{-2}

Fig. 10b

Fig. 10—Stress increment $\sigma_f - \sigma_y$ versus $\varepsilon^{\frac{1}{2}}$ for two phase Fe-Ta alloys (a) alloys 1, 2, and 3 (b) alloys 4 and 5.

-47-

R. H. Jones
m.m. - a.c. 3/1/73

Fig. 11—Stress increment $\sigma_f - \sigma_y$ versus the dimensionless parameter, $\left(bf\varepsilon/\bar{D}\right)^{\frac{1}{2}}$ for two phase Fe-Ta alloys at true plastic strains of 0.01, 0.025, and 0.050.